In studies by Nandi et al., HA-coated substrates provide direct evidence that CD44 plays a major role in regulating cell activity. The molecules of HA in HA-coated dishes effectively may bind to CD44 and RHAMM as a widely expressed cell surface receptor for HA.[19–21] In spite of the inhibitory effects on the GJIC in HMW HA-added dishes, we have found that the functional gap junction is promoted by HMW HA coating. Consequently, these results give useful information on how to design biomaterials of polysaccharides such as HA when the GJIC function is used as a marker for evaluating biocompatibility.[18]

CONCLUSIONS

In this study, the cell adhesion and cell function of GJIC were compared on dishes treated with various molecular weights of HA. The extent of attachment of NHDF cells on the HA-coated surfaces decreased linearly proportional to the MW size of HA at an early time point in the culture. Increasing HA MW suggests that HMW HA contributes to enhancing the hydrophilic property of its surface.

The SLDT method was used to study the effects of HA on the GJIC of NHDF cells. The results indicate that NHDF cells on dishes coated with HA in HMW (800 kDa) promote GJIC. However, the addition of HMW HA showed the opposite effect. Nutrients that promote the formation of the gap junction, such as bFGF,[8] EGF,[22] and TGF-β,[23] could be enveloped in the molecule of the coated HMW HA. In the case of LMW HA, the inhibitory effect of gap formation was not observed. In conclusion, it is suggested that the selection of the MW of HA is an important factor in designing biocompatible artificial skins that retain and enhance the function of GJIC in NHDF cells.

References

1. Greco RM, Iocono JA, Ehlich HP. Hyaluronic acid stimulates human fibroblast proliferation within a collagen matrix. J Cell Physiol 1998;177:465–473.
2. Martine C, Huong AN, Charles BU. The hyaluronan receptor (CD44) participates in the uptake and degradation of hyaluronan. J Cell Biol 1992;116:1055–1062.
3. Kawasaki K, Ochi M, Uchio Y, Adachi N, Matsusaki M. Hyaluronic acid enhances proliferation and chondroitin sulfate synthesis in cultured chondrocytes embedded in collagen gels. J Cell Physiol 1999;179:142–148.
4. Alaish SM, Yager DR, Diegelmann RF, Cohen IK. Hyaluronic acid metabolism in keloid fibroblasts. J Pediatric Surg 1995;30: 949–952.
5. El-fouly MH, Trosko JE, Chang CC. Scrape-loading and dye transfer: A rapid and simple technique to study gap junctional intercellular communication. Exp Cell Res 1987;168:422–430.
6. Zoelen EJ, Tertoolen LJ. Transforming growth factor-β enhances the extent of intercellular communication between normal rat kidney cells. J Biol Chem 1991;266:12075–12081.
7. Upham BL, Yao JJ, Trosko JE, Masten SL. Determination of the efficacy of ozone treatment systems using a gap junction intercellular communication bioassay. Environ Sci Technol 1995;29: 2923–2928.
8. Abdullah KM, Lutha G, Bilski JJ, Abdullah SA, Reynolds LP, Redmer DA, Grazul-Bilska AT. Cell-to-cell communication and expression of gap junctional proteins in human diabetic and nondiabetic skin fibroblasts. Endocrine 1999;10:35–41.
9. Siddiqui MU, Benatmane S, Zachayus JL, Plas C. Gap junctional communication and regulation of the glycogenic response to insulin by cell density and glucocorticoids in cultured fetal rat. Hepatocytes 1999;29:1147–1155.
10. Cowman MK, Li M, Balazs EA. Tapping mode atomic force microscopy of hyaluronan extend and intermolecularly interacting chains. Biophys J 1998;75:2030–2037.
11. Jacoboni I, Valdre U, Mori G, Quaglino JD, Ronchetti IP. Hyaluronic acid by atomic force microscopy. J Struct Biol 1999; 126:52–58.
12. Cramer JA, Bailey LC, Bailey CA, Miller RT. Kinetic and mechanistic studies with bovine testicular hyaluronidase. Biochim Biophys Acta 1993;1200:315–321.
13. Goegan P, Johnson G, Vincent R. Effects of serum protein and colloid on the alamarBlue assay in cell cultures. Toxicol In Vitro 1995;9:257–266.
14. Forrester JV, Balazs EA. Inhibition of phagocytosis by high molecular weight hyaluronate. Immunology 1980;40:435–446.
15. Lapcik JL, Lapcik L, Smedt SD, Demeester J, Chabrecek P. Hyaluronan: Preparation, structure, properties, and applications. Chem Rev 1998;98:2663–2684.
16. Albright CD, Grimley PM, Jones RT, Fontana JA, Keenan KP, Resau JH. Cell-to-cell communication: A differential response to TGF-β in normal and transformed (BEAS-2B) human bronchial epithelial cells. Carcinogenesis 1991;12:1993–1999.
17. Pepper MS, Meda P. Basic fibroblast growth factor increases junctional communication and connexin 43 expression in microvascular endothelial cells. J Cell Physiol 1992;153:196–205.
18. Tsuchiya T. A useful marker for evaluating tissue-engineered products: Gap-junctional communication for assessment of the tumor-promoting action and disruption of cell differentiation in tissue-engineered products. J Biomater Sci, Polym Edn 2000; 11:947–959.
19. Alaish SM, Yager DR, Diegelmann RF, Cohen IK. Hyaluronic acid metabolism in keloid fibroblasts. J Pediatric Surg 1995;30: 949–952.
20. Abetamann V, Kern HF, Elsasser HP. Differential expression of the hyaluronan receptors CD44 and RHAMM in human pancreatic cancer cells. Clin Cancer Res 1996;2:1607–1618.
21. Kawashima H, Hirose M, Hirose J, Nagakubo D, Plaas AH, Miyasaki M. Binding of a large chondroitin sulfate/dermatan sulfate proteoglycan, versican, to L-selectin, P-selectin, and CD44. J Biol Chem 2000;275:35448–35456.
22. Vikhamar G, Rivedal E, Mollerup S, Sanner T. Role of Cx43 phosphorylation and MAP kinase activation in EGF induced enhancement of cell communication in human kidney epithelial cells. Cell Adhes Commun 1998;5:451–460.
23. Van Zoelen EJJ, Tertoolen LGJ. Transforming growth factor-β enhances the extent of intercellular communication between normal rat kidney cells. J Biol Chem 1991;269:12075–12081.

Materials Transactions, Vol. 43, No. 12 (2002) pp. 3128 to 3130
Special Issuse on Biomaterials and Bioengineering

Tumor-Promoting Activity of 48 kDa Molecular Mass Hyaluronic Acid

Jeong Ung Park and Toshie Tsuchiya *

Division of Medical Devices, National Institute of Health Sciences, Tokyo 158-8501, Japan

Hyaluronic acid (HA), glycosaminoglycan, has long been implicated in malignant transformation and tumor-promoting activity. We found that 48 kDa molecular mass HA *in vitro* promotes tumor cell growth and tumorigenesis. The increase of cell growth rate in human hepatoma cells (HepG2 cells, cancer cells) and normal human dermal fibroblasts (NHDF cells, normal cells) treated with 48 kDa HA at 2×10^{-4} kg/L concentration were $110 \pm 0.9\%$ and $103 \pm 0.5\%$, respectively. Colony formation activity of 4.8 kDa HA in cultured Balb/3T3 clone A3111 cells was higher than that of 48 kDa HA. However, transforming activity of HA was significantly showed in 48 kDa HA but not in 4.8 kDa HA. These findings suggest that 48 kDa HA has a tumor-promoting activity stronger than 4.8 kDa HA, because the former increase the cell growth of cancer cells than the latter. The increase of cell growth rate in HepG2 cells (cancer cells) and NHDF cells (normal cells) were compared among various molecular masses of HA.

(Received May 20, 2002; Accepted July 19, 2002)

Keywords: *hyaluronic acid, tumorigenesis, colony formation activity, cell transformation, normal human dermal fibroblasts, human hepatoma cells*

1. Introduction

Hyaluronic acid (HA) is a non-sulfated glycosaminoglycan (GAG) that promotes motility, adhesion, and proliferation in mammalian cells, as mediated by cell-surface HA receptors.[1,2] Various tumors accumulate HA that suggested to facilitate tumor growth and invasion into the extracellular matrix (ECM) by a hydrodynamic effect, or by altering tumor cell behavior. Hyaluronidase (HAase) degrades HA into small fragments.[3] Decomposing HA into small fragment may result in the release of some cytokines which may promote the tumor growth and angiogenesis. Lokeshwar *et al.* reported that small fragments HA (3–25 disaccharide units) levels increased in prostate cancer tissues when compared with normal tissues.[4] Moreover, HA and its receptor, RHAMM (receptor for hyaluronic acid mediated motility) are important regulators of cell movement, adhesion and cytoskeletal organization. HA and RHAMM have been implicated in transformation and metastasis, in particular the processes of tumor cell motility and invasion.[5–9]

In the present study, we survey the growth rate of human hepatoma cells (HepG2 cells) and normal human dermal fibroblasts (NHDF cells), and promoting activity of HA is also confirmed by the *in vitro* two-stage transformation assay. These results provide the important evidence for a direct relationship between HA and tumorigenesis in tumor cells.

2. Materials and Method

2.1 Materials

AlamarBlue™ agent was purchased from Biosource (Camarillo, CA). Giemsa's solution was obtained from Merck (Germany). Hyaluronic acids (Fig. 1) (HA: 48 kDa and 800 kDa) were kindly supplied by Seikagaku Industries, Ltd. (Tokyo, Japan). HA of 4.8 kDa was prepared using the method of Cramer and coworkers.[10] All other chemicals of a special grade were used without further purification.

*Corresponding author: E-mail: tsuchiya@nihs.go.jp

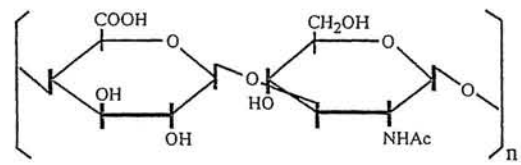

Fig. 1 Chemical structures of hyaluronic acid.

2.2 Cell cultures

Normal human dermal fibroblasts, NHDF cells (Asahi Techno Glass, Tokyo, Japan), and HepG2 cells (human hepatoma cell line, ATCC No.: HB-8065) were cultured in Dulbecco's modified Eagle's medium (DMEM; GIBCO BRL) supplemented with 10% heat-inactivated fetal calf serum (FCS; GIBCO BRL) and antibiotics [penicillin (100 unit/ml)-streptomycin (1×10^{-4} kg/L)]. Balb/3T3 clone A3111 cells (Dr. T. Kuroki, University of Tokyo) were cultured in MEM supplemented with 10% heat-inactivated fetal calf serum (FCS; GIBCO BRL). The media were changed every two days until the cells became confluent. NHDF and A3111 cells cultured between 4th and 9th passage levels were used for all experiments. Cell cultures were maintained in a humidified 5% CO_2 incubator at 37°C.

2.3 Cell proliferation assay

For measurement of cell proliferation, 8×10^4 cells (NHDF and HepG2) were seeded into 12-well culture plates. Solutions of various molecular masses of HA then were added to each culture well. After 4 days of HA-treatment, the extent of cell growth was measured by alamarBlue™ assay.[11] Control cells received fresh medium without any additions.

2.4 Transformation assay

For standard and two-stage cell transformation, 1×10^4 cells were plated per 60-mm tissue culture dish; 15 dishes were used for each point in all cell transformation experiments.[12,13] After 24 h, 1×10^{-7} kg/L 3-methylcholanthrene (MCA) was added to the MEM medium containing 10% FCS, and 72 h later the culture medium containing 4.8 kDa HA or

48 kDa HA was changed. The medium was changed twice a week for 6 weeks. The cells were fixed with formaldehyde and stained with 5% Giemsa solution for 12 h. Types of transformed focus were determined under a phase-contrast photomicroscope.

Colony-formation efficiency was tested in parallel with the transformation assay by seeding 100 cells/60-mm dish, and by treating the cells with the culture medium containing various molecular masses of HA and MCA for 72 h. The cultures were fixed and stained with 3% Giemsa solution, after 10–11 days from cell seeding, and colonies were counted. Each assay was repeated two times. Statistical analysis was carried out by the Wilcoxin Signed Rank Test.[14]

3. Results and Discussion

Results of the cell growth assays are given in Fig. 2. AlamaBlue™ assay indicated that cell proliferation capacities in the NHDF cells and HepG2 cells have different. The growth rate of HepG2 cells was accelerated after co-culture with 48 kDa HA at the concentration of 2×10^{-4} kg/L. However, 48 kDa HA had a low effect on growth rate of NHDF cells (Fig. 2(a)). These findings may related with reports that HA fragments by degrading enzyme HAase are intricately associated with cancer angiogenesis and metastasis.[15,16]

We surveyed the promoting activity of HA using an *in vitro*, two-stage transformation assay. Morphology of A3111 cells treated with MCA, 4.8 kDa HA and 48 kDa HA were observed by phase contrast photomicroscope after culture for 6 weeks. Figure 3 shows a photograph of Giemsa staining plates tested by the cell transformation method. As shown in Figs. 3(b) and (c), transformed foci was observed in the dishes of 4.8 kDa HA (b) and 48 kDa HA (c) at MCA concentration of 1×10^{-7} kg/L, respectively. When A3111 cells were treated with 48 kDa HA, the number of the transformed foci increased in comparison with 4.8 kDa HA as shown in

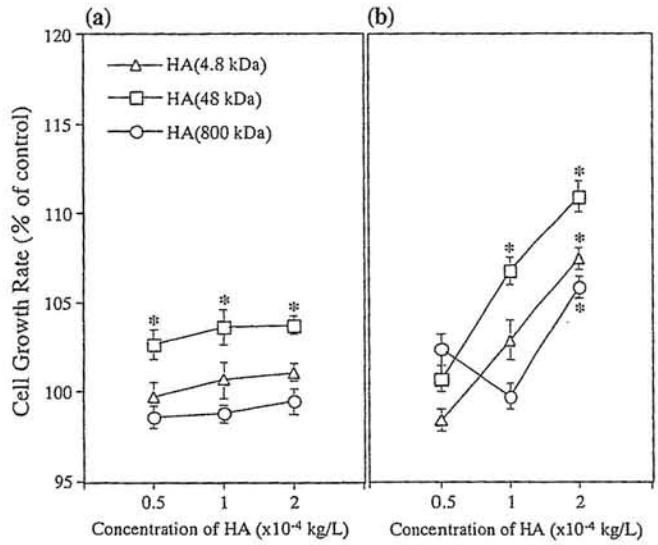

Fig. 2 Effect of various molecular weights of HA on NHDF cells or HepG2 cells growth. (*$p < 0.05$, Wilcoxin Signed Rank Test): (a) NHDF cells, (b) HepG2 cells.

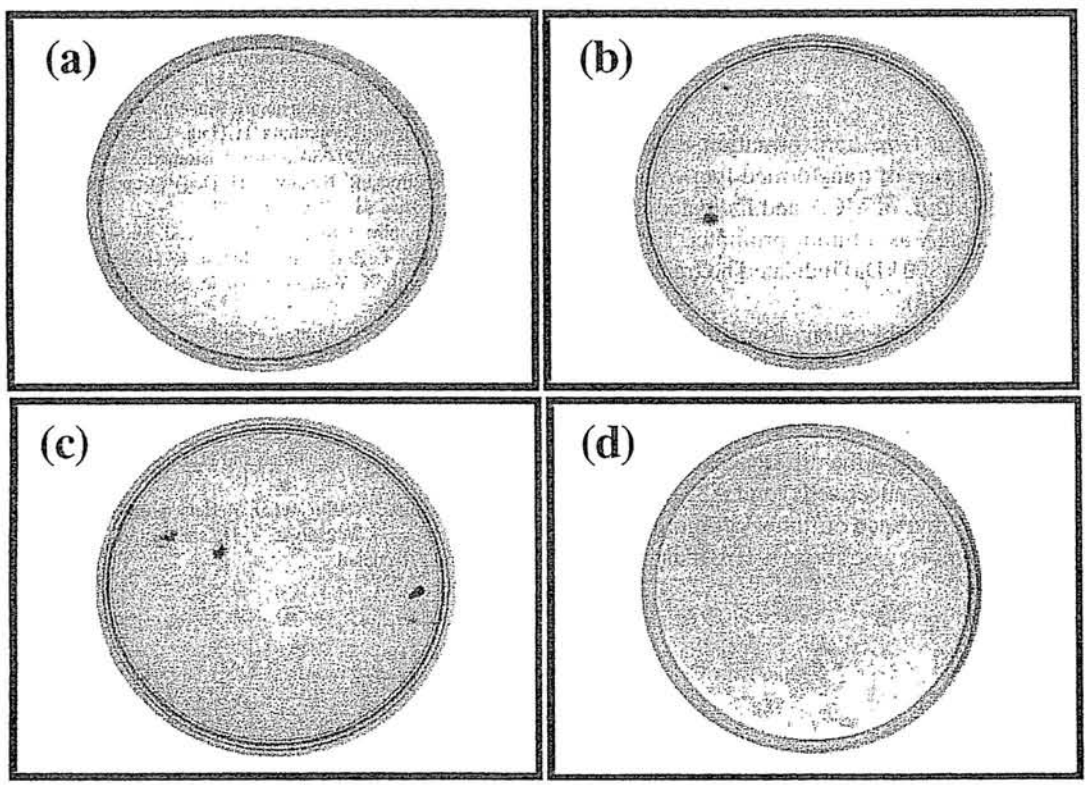

Fig. 3 Images of A3111 cells transformation on the 60-mm tissue culture dish initiated by MCA: (a) MCA of 1×10^{-4} kg/L from cell culture 1 day to 4 days, (b) MCA of 0.1 μg/mL from cell culture 1 day to 4 days and HA (4.8 kDa) of 10×10^{-4} kg/L from cell culture 7 days to 21 days, (c) MCA of 1×10^{-4} kg/L from cell culture 1 day to 4 days and HA (48 kDa) of 10×10^{-4} kg/L from cell culture 7 days to 21 days, (d) MCA of 0.1 μg/mL from cell culture 1 day to 4 days and HA (800 kDa) of 10×10^{-4} kg/L from cell culture 7 days to 21 days.

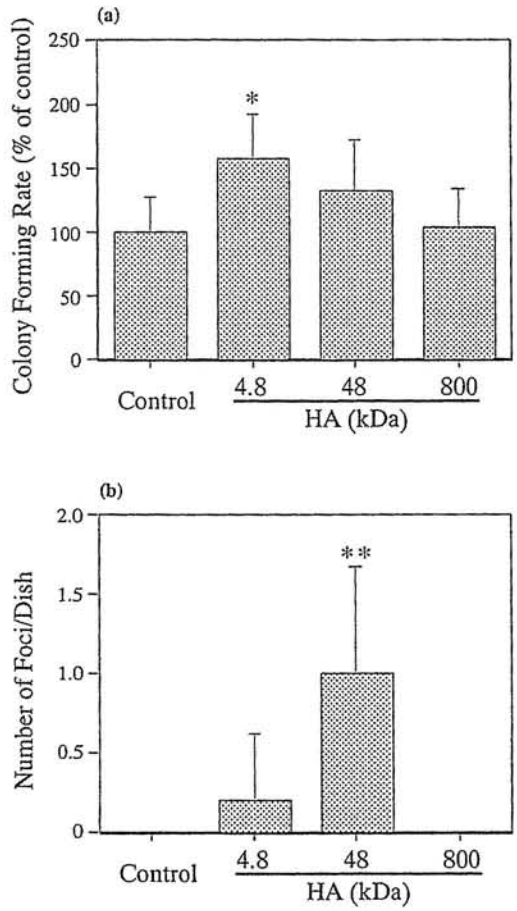

Fig. 4 Influence of HA on the colony formation activity and transformation of A3111 cells initiated by MCA (1×10^{-4} kg/L). A significant increase of transformed foci, in comparison with controls, is indicated ($^{*}p < 0.05$, $^{**}p < 0.01$, Wilcoxin Signed Rank Test): (a) colony forming rates after 2 weeks, (b) two-stage transformation assay.

Fig. 4(b). As a result, *in vitro* transformation experiments showed a significant increase of transformed foci with an initiating dose of 1×10^{-7} kg/L of MCA and indicated the possible activity of 48 kDa HA as a tumor promoter.[4,17,18] The high molecular mass HA (800 kDa) indicated no transforming activity as shown in Fig. 4(b).

As shown in Fig. 4(a), A3111 colony formation activity of 4.8 kDa HA was higher than that of 48 kDa HA. However, Fig. 2 indicated a slightly higher cell growth in 48 kDa HA than 4.8 kDa HA, in the case of HepG2 cells. These results were considered to be caused by the differences of cell functions between HepG2 cells (cancer cells) and A3111 (normal cells). It seems that the difference of tumor-promoting activity among the different molecular sizes of HA must be considered for the protection of the tumorigenesis, especially at the doubtful site of tumors.[19–21]

In the future, studies to define functional relationship between various molecular masses of HA and tumor cell properties are needed in order to provide insights into regulatory mechanisms involved in cell transformation in the tumor progression.

4. Conclusion

The 48 kDa HA indicated stronger tumor-promoting activity in transformation assay than high molecular mass HA (800 kDa) or low molecular mass HA (4.8 kDa) *in vitro*. These findings suggest that transformation of A3111 cells can be induced by 48 kDa HA, thus, degradable HA is useful index for early diagnosis of various cancers.

REFERENCES

1) T. C. Laurent and J. R. Fraser: FASEB J. **6** (1992) 2397–2404.
2) J. L. Lapcik, L. Lapcik, S. D. Smedt, J. Demeester and P. Chabrecek: Chem. Rev. **98** (1998) 2663–2684.
3) R. Stern, S. Shuster, T. S. Wiley and B. Formby: Exp. Cell Res. **266** 167–176.
4) V. B. Lokeshwar, D. Rubinowicz, G. L. Schroeder, E. Forgacs, J. D. Minna, N. L. Block, M. Nadji and B. L. Lokeshwar: J. Biol. Chem. **276** (2001) 11922–11932.
5) V. Assmann, J. F. Marshall, C. Fieber, M. Hofmann and I. R. Hart: J. Cell Sci. **111** (1998) 1685–1694.
6) J. Lesley, V. C. Hascall, M. Tammi and R. Hyman: J. Biol. Chem. **275** (2000) 26967–26975.
7) L. Y. Bourguignon, H. Zhu, B. Zhou, F. Diedrich, P. A. Singleton and M. C. Hung: J. Biol. Chem. **276** (2001) 48679–48692.
8) N. Iida and L. Y. W. Bourguignon: J. Cell. Physiol. **171** (1997) 152–160.
9) R. K. Chiu, A. Droll, S. T. Dougherty, C. Carpenito, D. L. Cooper and G. J. Dougherty: Exp. Cell Res. **248** (1999) 314–321.
10) J. A. Cramer, L. C. Bailey, C. A. Bailey and R. T. Miller: Biochim. Biophys. Acta. **1200** (1993) 315–321.
11) P. Goegan, G. Johnson and R. Vincent: Toxic *In Vitro* **9** (1995) 257–266.
12) T. Tsuchiya, K. Fukuhara, H. Hata, Y. Ikarashi, N. Miyata, F. Katoh, H. Yamasaki and A. Nakamura: J. Biomed. Mater. Res. **29** (1995) 121–126.
13) T. Tsuchiya, R. Nakaoka, H. Degawa and A. Nakamura: J. Biomed. Mater. Res. **31** (1996) 299–303.
14) C. L. Shapiro, J. Keating, J. E. Angell, M. Janicek, R. Gelman, D. Hayes and M. S. LeBoff: Cancer Invest. **17** (1999) 566–574.
15) R. Kosaki, K. Watanabe and Y. Yamaguchi: Cancer Res. **59** (1999) 1141–1145.
16) N. S. Chang, N. Pratt, J. Heath, L. Schultz, D. Sleve, G. B. Carey and N. Zevotek: J. Biol. Chem. **276** (2001) 3361–3370.
17) T. Asplund and P. Heldin: Cancer Res. **54** (1994) 4516–4523.
18) M. Culty, M. Shizari, E. W. Thompson and C. B. Underhill: J. Cell Physiol. **160** (1994) 275–286.
19) D. J. Beech, A. K. Madan and N. Deng: J. Surg. Res. **103** (2002) 203–207.
20) A. Thylen, J. Wallin and G. Martensson: Cancer. **86** (1999) 2000–2005.
21) K. Isama, A. Matsuoka, Y. Haishima and T. Tsuchiya: Mater. Trans. (2002) Accepted.

Neuro
-endocrinology

Neuroendocrinology 2002;76:223–234
DOI: 10.1159/000065948

Received: October 22, 2001
Accepted after revision: June 13, 2002

Effects of 17β-Estradiol and Xenoestrogens on the Neuronal Survival in an Organotypic Hippocampal Culture

Kaoru Sato[a] Norio Matsuki[b] Yasuo Ohno[a] Ken Nakazawa[a]

[a]Division of Pharmacology, National Institute of Health Sciences, and [b]Laboratory of Chemical Pharmacology, Graduate School of Pharmaceutical Sciences, University of Tokyo, Japan

Key Words

Xenoestrogens · Hippocampus · Glutamate · Gonadal steroids · Gonadal steroid antagonists · Gonadal steroid receptors · Immunocytochemistry · Bisphenol · Apoptosis

Abstract

Xenoestrogens are man-made compounds that mimic the actions of estrogens through interactions with estrogen receptors (ERs). Although xenoestrogens have received a great deal of attention as possible causes of brain disfunctions, little information concerning the effects of xenoestrogens on the central nervous system is available. In this study, we investigated the effects of 17β-estradiol (E_2) and four xenoestrogens (17α-ethynylestradiol, diethylstilbestrol, *p*-nonylphenol and bisphenol A (BPA)) on the neuronal survival using organotypic hippocampal slice cultures. When the cultured hippocampal slices were exposed to glutamate (1 m*M*, 15 min), the CA1-selective neuronal damage was induced. Pretreatment with E_2 and the xenoestrogens (24 h) selectively exacerbated the CA3 neuronal damage caused by glutamate. In spite of the marked difference of binding affinities to ERs, all compounds revealed maximal effects at 1 n*M*. ER antagonists, tamoxifen and ICI 182,780, did not affect responses to E_2 and the xenoestrogens, indicating that these effects are mediated through mechanisms other than ERs. In spite of the fact that BPA has little interaction with ERs at 1 n*M*, E_2 and BPA equally increased the expression of N-methyl-*D*-aspartate receptor in CA3 and upregulated the spine density of the apical portion of CA3 dendrites at 1 n*M*. These compounds also enhanced the sprouting of mossy fibers to CA3 neurons. These results suggest that exposure to E_2 and xenoestrogens during the developmental stage results in a marked influence on synaptogenesis and neuronal vulnerability through mechanisms other than ERs.

Introduction

Xenoestrogens are nonsteroidal, man-made compounds that enter our body by ingestion or adsorption, and mimic the actions of estrogens through interactions with estrogen receptors (ERs). Xenoestrogens include a number of substances such as pesticides and industrial byproducts. Because it was reported that preschool children who had been exposed to pesticides demonstrated disadvantages in eye-hand coordination and 30-min memory [1], xenoestrogens have received a great deal of attention as possible causes of brain dysfunctions. However, little information concerning the effects of xenoestrogens on

KARGER
Fax + 41 61 306 12 34
E-Mail karger@karger.ch
www.karger.com

0028–3835/02/0764–0223$18.50/0

Accessible online at:
www.karger.com/journals/dsu

Kaoru Sato, PhD
Division of Pharmacology
National Institute of Health Sciences
1-18-1 Kamiyoga, Setagaya-ku, Tokyo 158-8501 (Japan)
Tel. +81 3 3700 1141 (ext. 348), Fax +81 3 3707 6950, E-Mail kasato@nihs.go.jp

the central nervous system (CNS) is available. In the CNS, both ERα and ERβ are widely expressed and estrogens are thought to have diverse roles in regulating the structures and the functions of neuronal systems [2–5]. In addition to well-known ER-mediated genomic actions, recent reports show that estrogens have nongenomic effects on neuronal cells through mechanisms other than ERs [6–8]. It is possible that xenoestrogens also have similar diverse effects on the CNS neurons.

To investigate the effects of 17β-estradiol (E_2) and xenoestrogens on CNS neurons during development, we employed organotypic hippocampal slice cultures. In contrast to dissociated neuron cultures, organotypic slice cultures maintain neuronal configurations and region-dependent cellular properties similar to those found in vivo [9, 10]. The most important example of such properties is that cultured hippocampal slices exhibit the selective vulnerability of CA1 neurons, i.e. CA1 neurons are selectively damaged by ischemic insults [11] and glutamate [12] in cultured hippocampal slices.

In this study, we investigated the effects of E_2 and four xenoestrogens [17α-ethynylestradiol (EE), an estrogen used for oral contraceptive pills; diethylstilbestrol (DES), a synthetic estrogen for preventing miscarriages; *p*-nonylphenol (PNP), the degradation product of surface active agents used as a supplement of resins; bisphenol (BPA), a content of canned food, dental sealants and composites] on neuronal survival in cultured hippocampal slices. We also investigated the effects of these compounds on the expression of N-methyl-*D*-aspartate (NMDA) receptors, spine density and mossy fiber sprouting, which may affect neuronal survival.

Materials and Methods

Organotypic Hippocampal Culture

Organotypic cultures of hippocampi were processed using the interface method [9] according to Sato and Matsuki [12]. Brains were rapidly removed from 8-day-old Wistar rat pups, and 200-μm-thick horizontal entorhino-hippocampal slices were made using a microslicer. The slices were maintained in cold Gey's balanced salt solution supplemented with 6.5 mg/ml glucose bubbled with 95% O_2 and 5% CO_2. The medial entorhino-hippocampal slices were placed on transparent membranes (Millicell-CM, Millipore, Bedford, Mass., USA), and set in 6-well tissue culture plates containing 0.7 ml of the culture media consisting of 50% minimal essential medium, 25% Hanks' balanced salt solution (HBSS), and 25% donor horse serum supplemented with 6.5 mg/ml glucose, 50 U/ml penicillin G potassium, and 100 μg/ml streptomycin sulfate. The slices were cultured at 37°C in a moist 5% CO_2 atmosphere and the culture media were changed every other day. All experiments were undertaken using hippocampal slices cultured for 10 days because we considered this the optimal time for using cultured hippocampal slices as models having similar properties to those observed in vivo. After slicing, hippocampal slices recover from the damage and complete the trisynaptic neuronal circuitry (DG → CA3 → CA1) by 10–14 days in vitro (DIV) [13]. Additional aberrant fiber projections from CA3 to DG are observed in the hippocampal slices cultured for >2 weeks [14].

Drug Treatment

E_2 and the xenoestrogens were dissolved at 10 m*M* in ethanol and added to the culture media to yield the final concentrations. The slices were incubated for 24 h with 1 ml of the media including these compounds. Tamoxifen (Sigma, St. Louis, Mo., USA) and ICI (Tocris, Ballwin, Mo., USA) were dissolved at 1 m*M* in ethanol and co-applied with E_2 at the final concentrations. Glutamate was dissolved at 100 m*M* in phosphate-buffered saline (PBS) and added to the media to yield the final concentrations. The media including glutamate (1 ml) was added to both above and below the membrane. The cultures were then incubated at 37°C for 15 min, washed 3 times with HBSS and again incubated with fresh media for 24 h for recovery. These procedures are based on the glutamate toxicity study by Sato and Matsuki [12].

Propidium Iodide Uptake Assay

Neuronal viability was determined by the propidium iodide (PI) uptake assay [12]. PI was dissolved at 500 μg/ml in PBS and added to the recovery media at 5 μg/ml. After the 24-hour incubation, the slices were washed 3 times with HBSS and the fluorescent images were obtained by confocal microscopy using a 4× objective.

Immunohistochemistry

The slices were washed 3 times with 2 ml PBS for 5 min and fixed with 4% paraformaldehyde (PFA) (Wako Pure Chemical, Osaka, Japan) in 0.1 *M* phosphate buffer (BP) for 30 min. After washing with PBS, the slices were treated with 0.3% Triton X-100 in PBS for 60 min at room temperature, and blocked with PBS containing 10% Block Ace (Dainippon-Seiyaku, Osaka, Japan) at 4°C overnight. They were then incubated with rabbit polyclonal IgG to 23 residue-synthetic peptide corresponding to the C-terminus of the rat NR1 subunit of NMDA receptor (Upstate Biotechnology, Lake Placid, N.Y., USA) diluted at 1:100 in the vehicle (PBS containing 10% Block Ace) for 8 h at 4°C. After wash, they were incubated with Alexa Fluor 488 goat anti-rabbit IgG (Molecular Probes, Eugene, Oreg., USA) diluted at 1:200 in the vehicle for 4 h at 4°C. After washing with PBS, fluorescent images were obtained by confocal microscopy using a 4× objective or a 60× oil immersion objective.

DiI Staining

The slices were washed 3 times with 2 ml PBS for 5 min and fixed with 4% PFA in 0.1 *M* PB for 30 min. The fixative above the membrane was removed and 1,1′-dioctadecyl-3,3,3′,3′-tetramethylindocarbocyanine perchlorate (DiI; Molecular Probes) crystals were embedded in CA1 and CA3 pyramidal cell layers under the microscope. After a 3-day incubation at room temperature, the morphology of the neurons was observed by confocal microscopy using a 60× oil immersion objective.

Confocal Microscopy

Fluorescent images were visualized by the μ-Radiance laser scanning confocal system (BioRad, Hercules, Calif., USA) equipped with an inverted microscope (Nikon, Tokyo, Japan). The slices were

observed using a 4× objective or a 60× oil immersion objective. Data of each session were collected at the same gain and black level settings. When the 60× objective was used, horizontal optical sections were taken at 10 μm steps and the resultant z-series were summed up to a flat image.

TSQ Staining

Mossy fiber terminals were visualized by staining of Zn^{2+} in the synaptic vesicles according to the modified protocol by Frederickson et al. [15]. A working solution of N-(6-methoxy-8-quinolyl)-*p*-toluenesulfonamide (TSQ) was prepared as follows. Sodium acetate (1.9 g) and sodium barbital (2.9 g) were dissolved in 100 ml of triple deionized water and 0.1 ml hot ethanol containing 1.5% TSQ was added. The working solution was made immediately before using and adjusted to pH 10.0. After wash with HBSS, the cultured slices were fixed with 8 ml of methanol for 10 min in Petri dishes. After treatment with 8 ml of acetone for 3 min, the slices were washed with PBS 3 times for 5 min and immersed in 8 ml of TSO working solution for 5 min. After wash with PBS, the slices were carefully removed from the membranes and placed on clean microscope slides. TSQ fluorescence (385 nm) emitted by excitation at 340 nm was digitally imaged by an inverted microscope equipped with an intensified charged-coupled device camera and a digital image processor (Argus 50/CA, Hamamatsu Photonics, Hamamatsu, Japan). Sixteen trial images obtained with a 4× objective were averaged to improve the signal-to-noise ratio.

Image Analysis

Image analysis was performed using a graphic software (Photoshop ver. 5.5, Adobe Systems, Mountain View, Calif., USA). For measuring the fluorescence intensity, five square windows (10,000 μm^2 each) were placed on desired regions, and the fluorescence intensity was obtained by measuring averaged gray-scale values of the selected windows. The intensities of these five windows were averaged and the background intensity was subtracted. In PI uptake experiments, data were normalized to 100% cell damage measured from the slices which had been exposed to 0.3% Triton X-100 for 4 h. In immunohistochemical staining and TSQ staining, the data are shown as averaged pixel intensities. Spines on the proximal sites of apical and basal dendrites were counted and the numbers per 10 μm are shown.

Statistical Analysis

The data were obtained from 4–8 independent experiments (averaged values of 4 slices for each), expressed as means ± SEM values. Tests of variance homogeneity, normality and distribution were performed to ensure that the assumptions required for standard parametric ANOVA were satisfied. Statistical analysis was performed by one-way repeated-measure ANOVA and post hoc Tukey's test for multiple pairwise comparisons.

Results

When applied alone, E_2 and the xenoestrogens (1 p*M* to 100 μ*M*, 24 h treatment) had no effect on neuronal viability in all regions of cultured hippocampal slices. However, these compounds markedly affected neuronal vulnerability to glutamate. Figure 1 shows the effect of E_2 on the glutamate toxicity in the cultured hippocampal slices. We visualized injured or dead cells by PI, which entered cells that had lost membrane integrity and emitted fluorescence when bound to nucleic acids. As shown in figure 1a (left) and 1b, glutamate (1 m*M*, 15 min) induced region-dependent neuronal damage (CA1 > CA3 > DG). Pretreatment with E_2 (24 h) markedly exacerbated the glutamate-induced neuronal damage in CA3 at 1 n*M* and higher concentrations [fig. 1a (right), b]. The maximal effect was observed at 1 n*M* (142.9% of the group exposed to glutamate alone) followed by a slight decline at higher concentrations. By contrast, E_2 attenuated the neuronal damage in CA1 at 1 p*M* and 1 n*M* (70.0 and 78.5% of the group exposed to glutamate alone, respectively).

The four xenoestrogens (EE, DES, PNP and BPA) also exacerbated the CA3 neuronal damage induced by glutamate (fig. 2). In contrast to their various binding affinities to ERs [16], all of these compounds produced maximal effects at 1 n*M* followed by declines at higher concentrations. DES (100 n*M*), PNP (1 n*M* to 100 μ*M*) and BPA (100 μ*M*) attenuated the neuronal damage in CA1. Although 1 n*M* DES and 1 μ*M* BPA exacerbated the CA1 and DG damage, these effects were weak compared with the effects stated above.

To examine the correlation between ERs and the exacerbation by E_2 and the xenoestrogens of CA3 damage, an ER antagonist, tamoxifen (100 n*M* to 10 μ*M*) or ICI (10 n*M* to 1 μ*M*) was co-applied with these compounds (table 1). We confirmed that neither of these antagonists alone affected the glutamate-induced damage. Neither tamoxifen nor ICI inhibited the effects of E_2 and the xenoestrogens, indicating that these compounds exacerbated CA3 neuronal damage through signaling pathways independent of ERs.

In ER-binding assays, the dissociation constants (Kd) of E_2 for ERα and ERβ are 0.1 and 0.4 n*M* [17]. BPA is the weakest estrogen among the xenoestrogens used in this report and requires 300- and 2,000-fold higher concentrations than E_2 for binding to ERα and ERβ, indicating that BPA has no interaction with ERs at 1 n*M*. Therefore, to clarify the cytoarchitectural changes underlying the increased vulnerability of CA3 neurons unrelated to ERs, we used 1 n*M* BPA as well as 1 n*M* E_2 and compared their effects on the expression of NMDA receptor, spine density and mossy fiber sprouting, which may affect the neuronal survival.

Figure 3 shows the effect of E_2 and BPA on expression of the NMDA receptor, identified by immunostaining of the NR1 subunit, which is indispensable for functional receptors [18, 19]. In control slices, the neuronal layers in

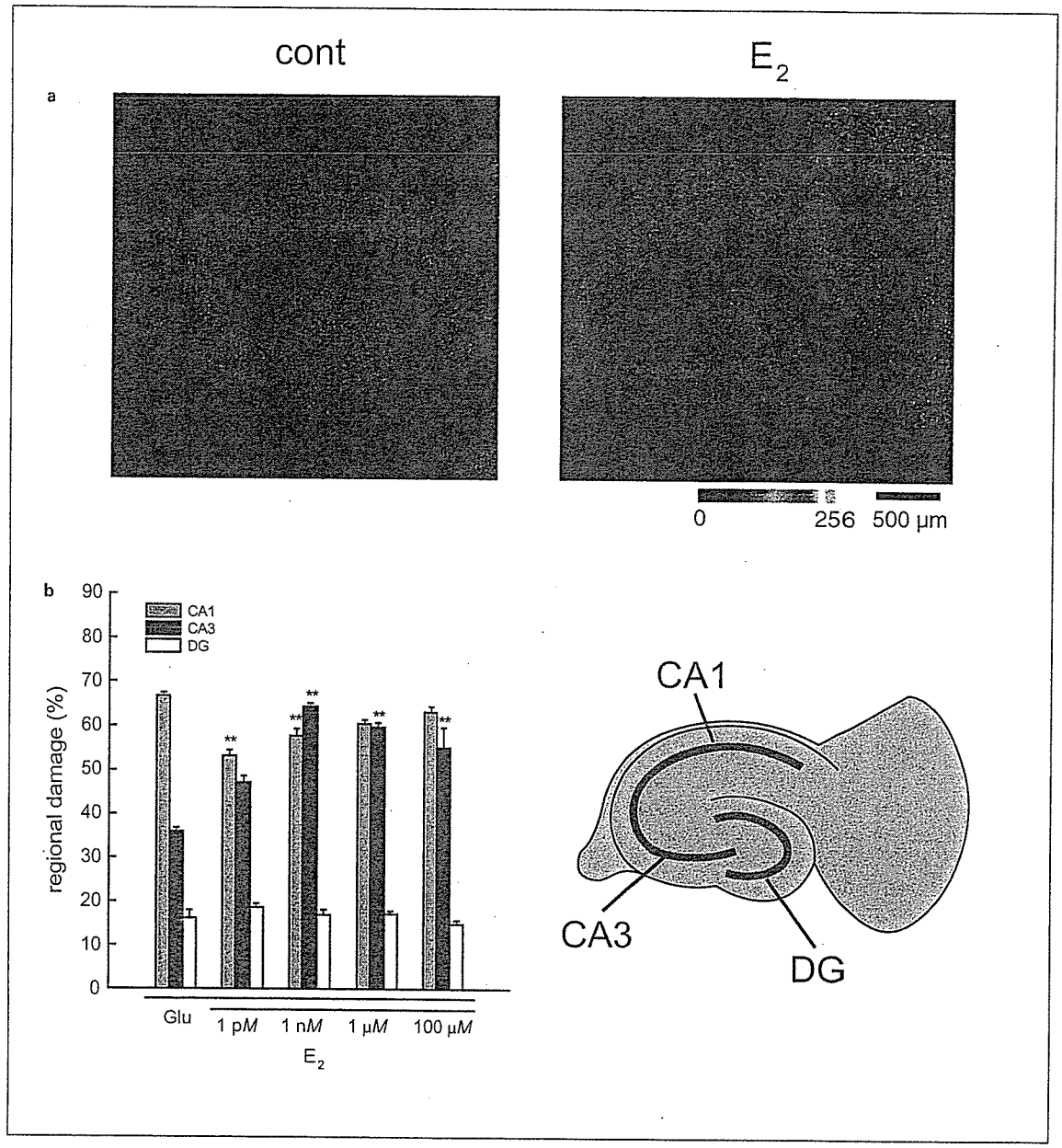

Fig. 1. The effect of E_2 on the glutamate-induced neuronal damage in the cultured hippocampal slice. **a** Typical PI fluorescent images of the slice exposed to glutamate alone (1 m*M*, 15 min, left) and the slice pretreated with E_2 (1 n*M*, 24 h) before the exposure to glutamate (right). **b** Normalized PI fluorescence intensities in CA1, CA3 and DG. E_2 selectively exacerbated the CA3 neuronal damage caused by glutamate and the most pronounced effect was observed at 1 n*M*. Experiments were repeated with 8 different plates, producing the same results. ** $p < 0.01$ vs. the group exposed to glutamate alone; n = 8, Tukey's test following ANOVA.

Fig. 2. The effects of EE (**a**), DES (**b**), PNP (**c**) and BPA (**d**) on the glutamate-induced neuronal damage in the cultured hippocampal slices. Normalized PI fluorescence intensities in CA1, CA3 and DG are shown. All of these compounds exacerbated the CA3 neuronal damage caused by glutamate and the most pronounced effect was observed at 1 n*M*. Experiments were repeated with 8 different plates, producing the same results. * $p < 0.05$; ** $p < 0.01$ vs. the group exposed to glutamate alone; n = 8, Tukey's test following ANOVA.

Table 1. Effects of ER antagonists on the exacerbation of the CA3 damage by E_2 and the xenoestrogens

	Exacerbation rate, %		
	– antagonists	+ antagonists	
		tamoxifen	ICI
Glutamate alone	100±7.28	110.24±8.99	118.888±8.95
+ E_2	227.68±15.42**	214.40±22.71	188.55±28.63
+ EE	195.22±9.13**	194.21±15.04	185.94±12.19
+ DES	177.05±14.74**	199.77±18.93	182.70±8.31
+ PNP	166.39±11.86**	196.75±18.93	171.58±18.15
+ BPA	179.84±14.39**	205.00±21.26	198.55±10.91

Tamoxifen (10 μ*M*) and ICI (1 μ*M*) did not affect the exacerbation of the CA3 damage by 1 n*M* of E_2 and xenoestrogens. ** $p < 0.01$ vs. the group exposed to glutamate alone; n = 4, Tukey's test following ANOVA.

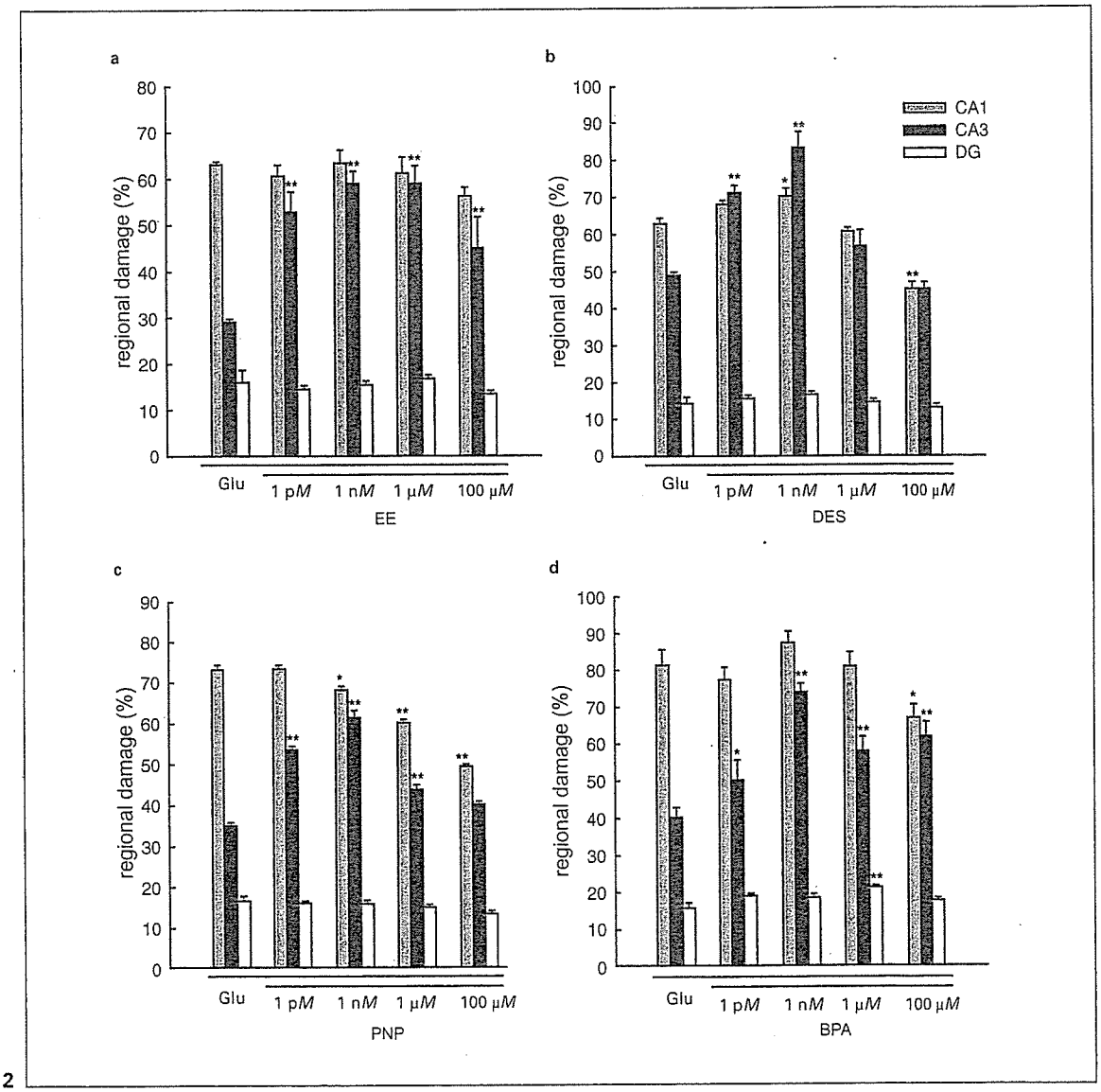

2

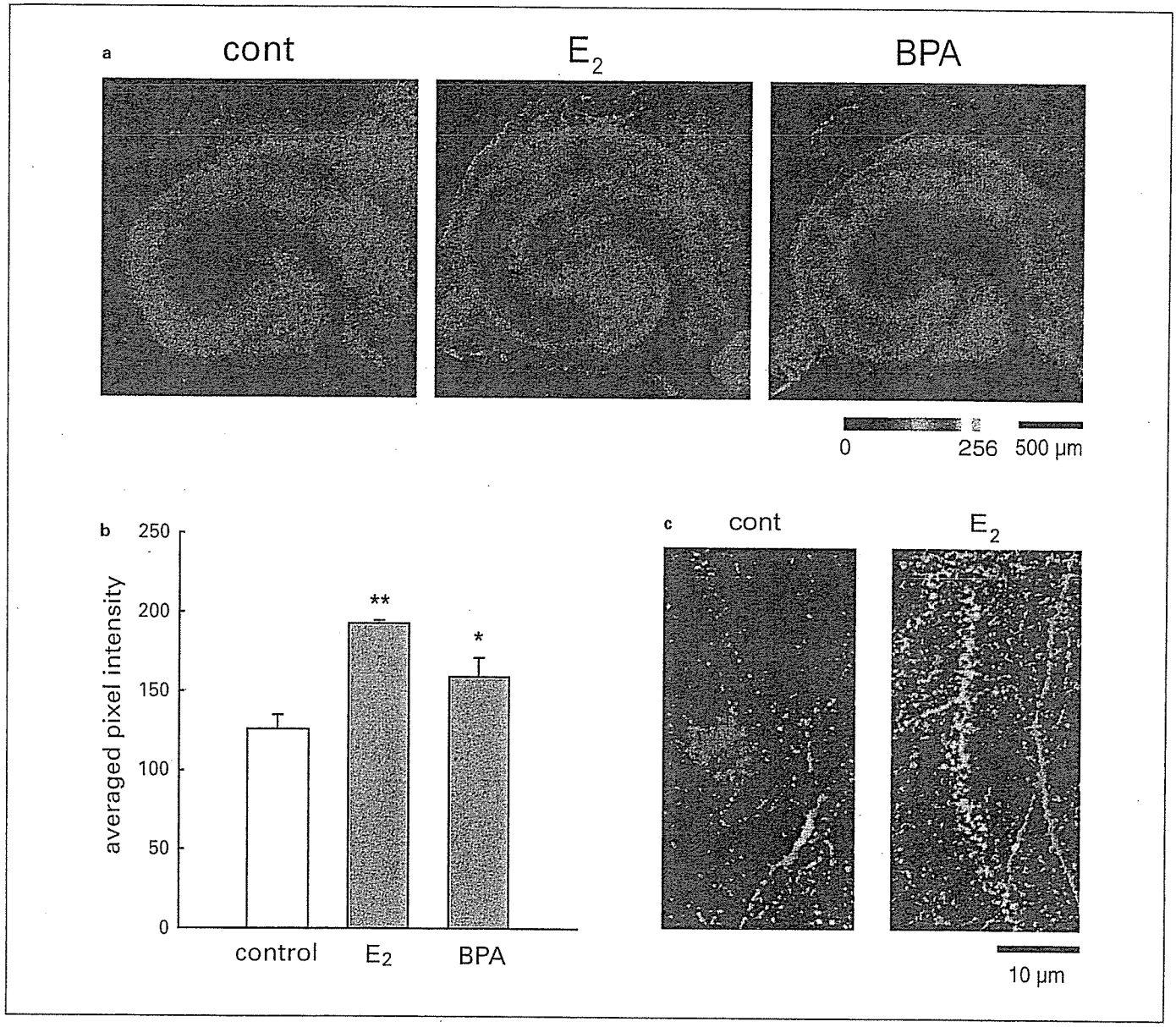

Fig. 3. The effects of E_2 and BPA (1 n*M*, 24 h) on the expression of NR1 subunit of NMDA receptor. **a** Typical NR1 immunofluorescence in the control slice (left), the slice treated with E_2 (middle) and the slice treated with BPA (right). **b** Normalized fluorescence intensity in CA3. E_2 and BPA significantly increased the expression of NR1. * $p < 0.05$; ** $p < 0.01$ vs. control group; n = 4, Tukey's test following ANOVA. **c** Typical fluorescent images of CA3 apical dendrites of the control slice (left) and the slice treated with E_2 (right), double-stained with DiI (red) and NR1 immunostaining (green). The induction of NR1 by E_2 on the CA3 apical dendrites was identified as yellow patches.

CA1, CA3 and DG were NR1 immunopositive, and the strongest signal was observed in CA1 (fig. 3a, left). After the exposure to E_2 and BPA (1 n*M*, 24 h), the CA3 signal was largely increased (152 and 133% of the control group, respectively; fig. 3a, b). Although increases were also observed in CA1 and DG, these changes were weak compared with that in CA3. A recent report has shown that the apical dendrites of CA3 neurons (stratum lucidum) scarcely express NR1 [20]. Thus, we confirmed the induction by E_2 of NR1 on the CA3 apical dendrites by double-staining with DiI (fig. 3c, red) and NR1 antibody (fig. 3c, green). Although NR1 signals were weak on the CA3 api-

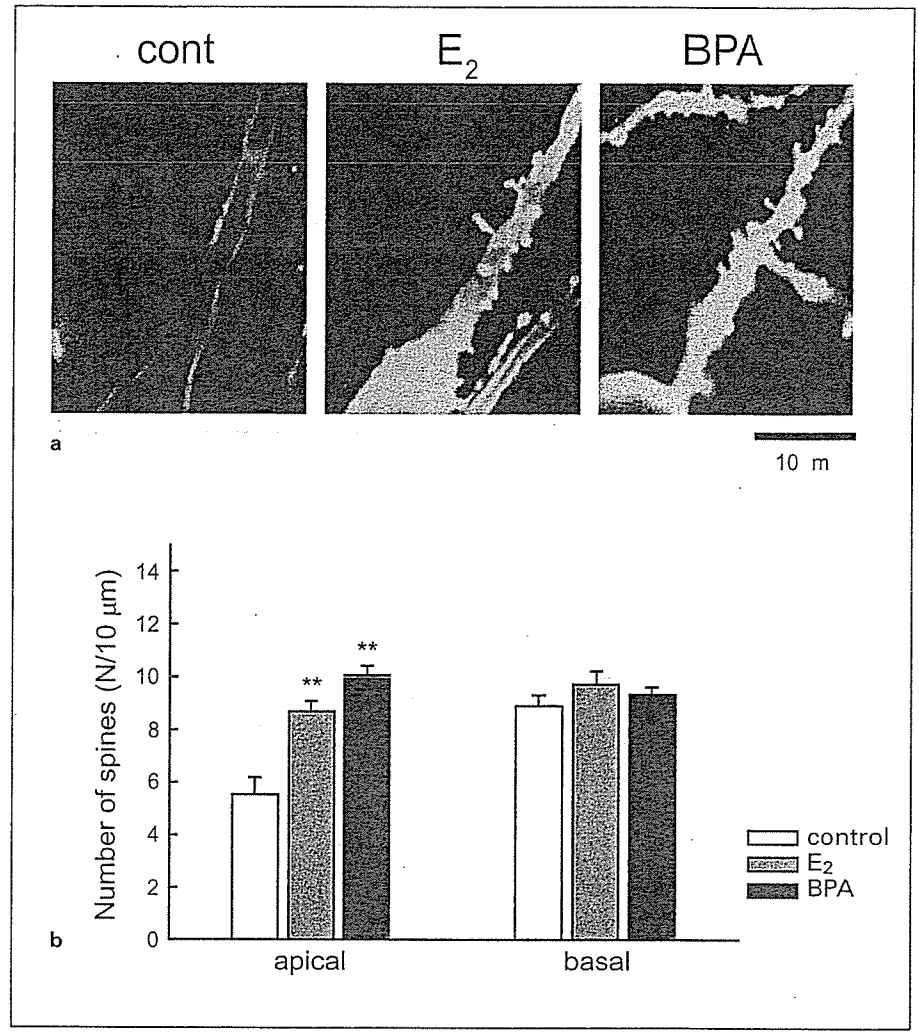

Fig. 4. Effects of E_2 and BPA (1 n*M*, 24 h) on spine density. **a** Typical fluorescent images of DiI-stained CA3 apical dendrites of the control slice (left), the slice treated with E_2 (middle) and the slice treated with BPA (right). **b** Spine density of the apical and basal dendrites of CA3 neurons. E_2 and BPA significantly increased the spine density of the apical dendrites. ** $p < 0.01$ vs. control group; n = 4, Tukey's test following ANOVA.

cal dendrites in the control slices (fig. 3c, left), the patchy yellow signals were found on CA3 apical dendrites in the E_2-treated slices (fig. 3c, right), indicating that these compounds promote the expression of NMDA receptor.

Spines were visualized by staining with DiI. E_2 and BPA (1 n*M*, 24 h) significantly increased the spine density of the apical portion of CA3 dendrites (158 and 187% of the control group, respectively), whereas they had no effect on that of the basal portion (fig. 4b). Typical morphologies of CA3 apical dendrites are shown in figure 4a. In CA1, these compounds had no effect on spine densities.

Mossy fiber terminals were visualized by using TSQ, a quinoline that emits strong fluorescence when it chelates to Zn^{2+} in synaptic vesicles. At first, we confirmed the specificity of TSQ to mossy fiber terminals (fig. 5). When the slices were stained with TSQ, the fluorescence was observed in the stratum lucidum of CA3 and in the hylus of DG (fig. 5a). When the slices were pretreated with dithizone, a nonfluorescent Zn^{2+} chelator, the TSQ fluorescence almost disappeared, indicating that TSQ emits fluorescence when it binds to endogenous Zn^{2+} (fig. 5b). When the slices whose DG region had been dissociated on DIV 1 were stained (fig. 5c), TSQ fluorescence in the stratum lucidum also disappeared (fig. 5b), indicating that this fluorescence is localized in the mossy fiber terminals. As shown in figures 6a and 6b, both E_2 and BPA increased the TSQ fluorescence in the stratum lucidum at 1 n*M* (161 and 131% of the control group, respectively), suggesting that these compounds enhance the sprouting of mossy fiber terminals. In addition, these compounds also enhanced the signal in the DG hilus.

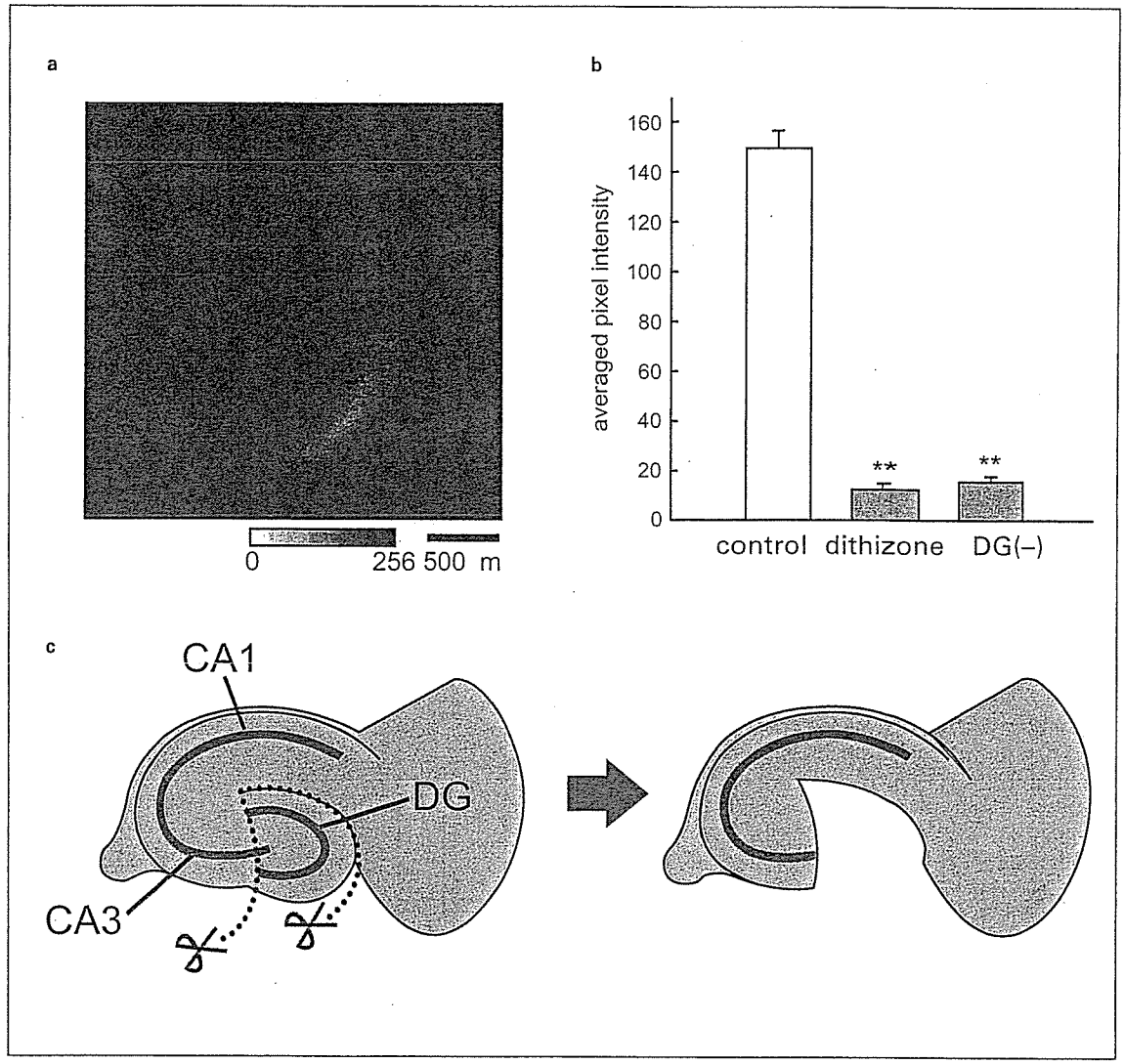

Fig. 5. TSQ emitted fluorescence in the stratum lucidum by binding to Zn^{2+} in the synaptic vesicles of mossy fiber terminals. **a** Typical TSQ fluorescence in the control slice. **b** Normalized TSQ fluorescence intensities of the slices pretreated with dithizone (1 m*M*) and the slices cultured without DG region. TSQ fluorescence disappeared by these treatments. ** $p < 0.01$ vs. control group; n = 6, Tukey's test following ANOVA. **c** The slice whose DG region was dissociated on DIV 1.

Discussion

We investigated the effects of E_2 and xenoestrogens on CNS neurons using organotypic hippocampal slice cultures. Our results are summarized as follows: (1) E_2 and xenoestrogens selectively exacerbated the CA3 neuronal damage caused by glutamate, (2) the effects were mediated through mechanisms other than ERs, (3) both E_2 and BPA increased the expression of NMDA receptor and the spine density of apical dendrites in CA3, and (4) E_2 and BPA enhanced the sprouting of mossy fiber terminals to CA3 neurons.

Little information is available concerning the effects of E_2 and xenoestrogens on CNS neurons during the postnatal developmental stage. Hippocampal slices were made from 8-day-old postnatal rats and cultured for 10 days with medium containing gelding horse serum, in which levels of estrogens were under the detection limit. It has been reported that during postnatal development, the capability of the estrogen-binding protein is high enough

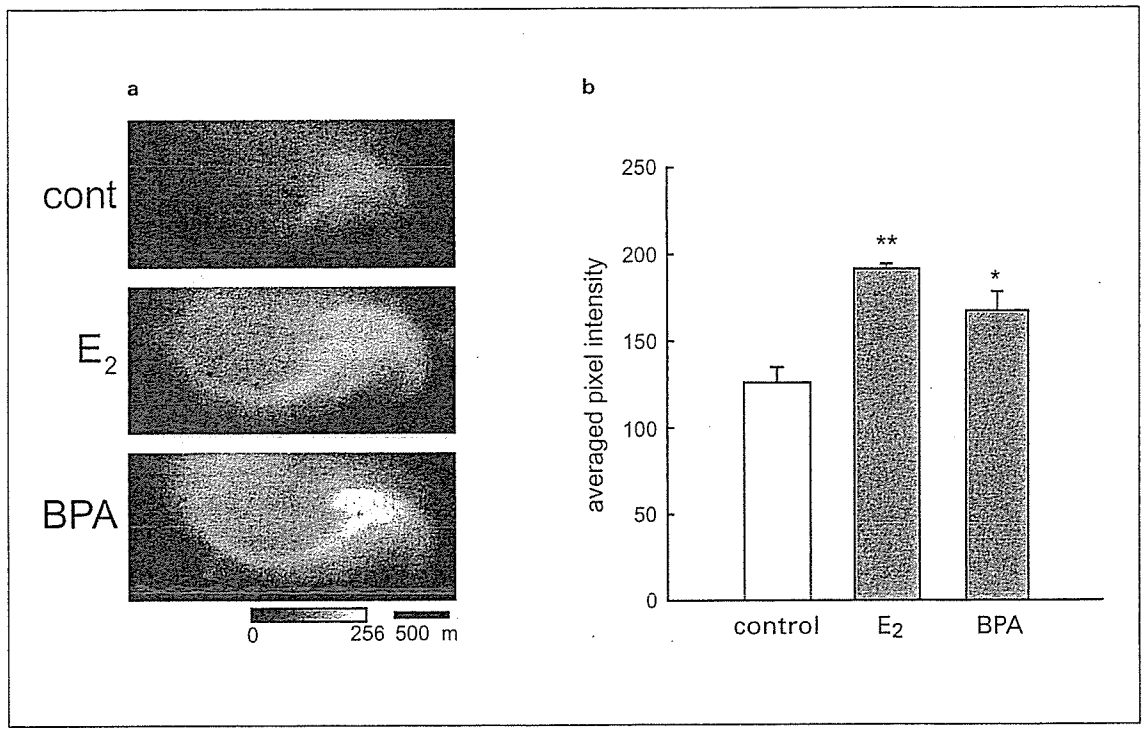

Fig. 6. The effects of E_2 and BPA (1 n*M*, 24 h) on the mossy fiber sprouting. **a** Typical TSQ fluorescence in the control slice (upper), the slice treated with E_2 (middle) and the slice treated with BPA (bottom). **b** Normalized TSQ fluorescence intensities in the stratum lucidum of CA3. E_2 and BPA significantly enhanced the mossy fiber sprouting. * $p < 0.05$; ** $p < 0.01$ vs. control group; n = 6, Tukey's test following ANOVA.

and the concentration of serum estrogens is lowered to nonphysiological levels [21]. Thus, our results can be regarded as the acute effects of xenoestrogens on the hippocampal neurons during postnatal development if these compounds can escape from the protein binding.

Although the four xenoestrogens used here have various binding affinities to ERs ($E_2 \fallingdotseq EE \fallingdotseq DES > PNP >$ BPA) [16], they similarly exacerbated the glutamate-induced CA3 damage with maximal effects observed at 1 n*M*. Saturation ligand binding analysis has revealed that the dissociation constants (Kd) of ERα and ERβ for E_2 are 0.1 and 0.4 n*M*, respectively [17]. BPA has the lowest binding affinities to ERs among the four xenoestrogens and its affinities to ERα and ERβ are 2,000 and 300 times lower than E_2 [17]. Thus, BPA has little interaction with ERα and ERβ at 1 n*M*, suggesting that these effects of E_2 and the xenoestrogens are independent of ERs. We confirmed this hypothesis using two ER antagonists of distinct classes, tamoxifen and ICI. Although tamoxifen is a partial agonist of ERs and mimics the agonistic effect of E_2 in some tissues [22], it has been reported that this compound completely antagonizes E_2 in the CNS neuron culture [23]. ICI is a pure antiestrogen and binds to ligand-binding domains of both ERα and ERβ [24]. Neither of these compounds affected the exacerbation by E_2 and the xenoestrogens of the CA3 damage, indicating that the effects were mediated through mechanisms other than ERs.

In contrast to CA3, CA1 damage was attenuated by E_2 and the xenoestrogens. Females are known to be less vulnerable to acute insults associated with cerebral ischemia, neurotrauma, hypoxia, and drug-induced toxicity [25]. In vitro studies also demonstrated that estrogens were protective against neuronal injury induced by excitatory amino acids, β-amyloid peptide or oxidative stress [26]. Optimal concentrations of E_2 for these protective effects vary from one report to the other suggesting that multiple mechanisms underlie them. The effects observed at low concentrations (p*M* to n*M*) are ER dependent [25], and relate to extracellular signal-regulated kinase (ERK) activation [27] and/or brain-derived neurotrophic factor (BDNF) induction [28]. On the other hand, the effects observed at concentrations higher than 1 μ*M* depend on the antioxidant activities and the hydrophobic phenolic molecules that

have the same chemical properties as E_2 and are also neuroprotective at this concentration [29]. In this study, only E_2 showed a protective effect at 1 p*M* and 1 n*M*, suggesting that this may have been mediated by ERs. Because part of glutamate neurotoxicity is caused by reactive oxygen species [30], neuroprotection by the xenoestrogens at higher concentrations than 1 μ*M* may have been due to their antioxidant activities. The antioxidant property of E_2 may have been masked by its ER-mediated effect. In addition, in CA3, the region-specific exacerbation may have prevailed over neuroprotective effects of these compounds.

As described above, E_2 and the xenoestrogens exacerbated the CA3 damage induced by glutamate without interaction with ERs. Because BPA has little interaction with ERα and ERβ at 1 n*M* owing to its low binding affinity [17], the common cytoarchitectural changes induced by E_2 and BPA in CA3 may correlate with this ER-unrelated increased vulnerability of CA3 neurons. Although various glutamate receptor subtypes are implicated in excitotoxic cell death, it is generally accepted that NMDA receptor plays a major role, mainly owing to its high Ca^{2+} permeability [31]. Thus, we examined the effects of E_2 and BPA on the expression of NR1, the obligatory subunit of the NMDA receptor function [18, 19]. Both compounds equally increased the expression of NR1 in CA3. In ovariectomized (OVX) adult rats, E_2 increases the expression of NMDA receptor in CA1 by posttranscriptional regulation [32]. In our study, E_2 and BPA had no effect on the NR1 expression in CA1, suggesting that the regulation by estrogens of the expression of NMDA receptor during the developmental stage is different from that in the adult period. Whether or not the effect during the developmental stage is also mediated by posttranscriptional regulation needs to be evaluated.

The increased level of NMDA receptor protein suggests that E_2 and BPA increase the number of synapses. Because dendritic spines are the major postsynaptic targets for excitatory synaptic inputs [33], we investigated the effect of E_2 and BPA on the spine density. The apical dendrites of CA3 pyramidal neurons receive mossy fibers at the proximal segment (stratum lucidum), entorhinal fibers at stratum moleculare, septohippocampal fibers at the middle and terminal dendritic regions (stratum radiatum) and other associational, commissural and collateral inputs in the middle segments. The basal dendrites receive mossy fiber collaterals, commissural and septal inputs at the proximal regions (stratum oriens) [34]. E_2 and BPA specifically increased the spine density at the proximal site of CA3 apical dendrite, suggesting that these compounds induced the synaptogenesis between CA3 neurons and mossy fibers. In OVX adult rats, E_2 upregulates the spine density of CA1 neurons via ERs [35] in an NMDA receptor-dependent manner [2]. It is possible that the increase in spine density in our study is also dependent on the NMDA receptor activity. However, the trigger causing the increase in CA3 spine density during the postnatal period are different from that in CA1 of adult rats because the effect was ER independent in our study. It is reported that cAMP response element binding protein (CREB) phosphorylation [36] and the decrease in GABAergic input [37] relate to the generation of new dendritic spines by E_2 in cultured hippocampal neurons. These steps may also correlate with the effects observed in our study.

Because increased spine density was observed specifically in the proximal site of CA3 apical dendrite corresponding to the postsynaptic site of mossy fiber-CA3 synapse, we next investigated the effects of E_2 and BPA on the presynaptic terminal density of mossy fibers by TSQ staining. In mossy fiber terminals, abundant Zn^{2+} is localized in the synaptic vesicles [38, 39]. Although the silver-amplification method (Timm-Danscher staining) has been widely used to stain Zn^{2+} in mossy fiber terminals, the possibility of labeling other heavy metals with this method has not been definitively excluded [15]. In the present study, we visualized Zn^{2+} with TSQ, a quinoline that forms Zn^{2+}, i.e. quinoline fluorescent chelates. Although Ca^{2+} and Mg^{2+} are also biologically relevant cations that form fluorescent complexes with TSQ [40], the binding constant of TSQ for Zn^{2+} is >1,000-fold higher than that for Ca^{2+} or Mg^{2+} [41]. We confirmed that the TSQ fluorescence completely disappeared when the slices had been pretreated with another nonfluorescent Zn^{2+} chelator, dithizone or TPEN. In addition, TSQ fluorescence in the stratum lucidum of the slice completely disappeared when the DG region had been dissociated on DIV 1. Based on these data, we supposed that the TSQ signals observed in this study represent Zn^{2+} in synaptic boutons of mossy fibers as has been reported [15]. Pretreatment with E_2 or BPA increased TSQ fluorescence in the stratum lucidum, indicating that sprouting or branching of mossy fiber terminals were induced by these compounds.

The upregulation of NMDA receptor, spine density and mossy fiber sprouting by E_2 and BPA suggest that these compounds enhance the synaptic reorganization of mossy fibers with CA3 neurons through mechanisms other than ERs. A series of changes observed in our study have much in common with those of epileptic hippocampus. Selective neuronal death in CA3 [42] and aberrant

sprouting of mossy fibers [43–45] have been described in the epileptic hippocampus. Afferent inputs strongly influence the shape and the number of dendritic spines [46–48]. The elevation of neuronal activity, like epilepsy, is generally thought to result in the upregulation of spines. Therefore, the synaptic reorganization in CA3 induced by E_2 and the xenoestrogens may contribute as key steps to increased vulnerability of CA3 neurons. Mossy fibers also establish synaptic contacts with polymorphic neurons in the DG hilus. The TSQ fluorescence observed in DG may represent a small population of recurrent axon collaterals branching from parent mossy fibers. Interestingly, E_2 and BPA increased the TSQ fluorescence in the hilus as well as that in the stratum lucidum of CA3, suggesting that these compounds directly enhance mossy fiber sprouting. There may be some additional factors that cause increased vulnerability of CA3, and the increased level of NMDA receptor may be one of such factors.

Recent studies have provided a large body of evidence that estrogens interact with plasma membrane binding sites/receptors, which are hypothesized to be of G-protein-coupled type and reveal the effects via cAMP/protein kinase A (PKA) signaling pathway [49]. Although the target site(s) of E_2 and the xenoestrogens still remain to be determined, the responses observed in the present study may be mediated through membrane binding sites/receptors coupled to intracellular transduction pathways. This is consistent with a report indicating that the generation of new dendritic spines requires phosphorylation of CREB [36].

Our results raise the possibility that exposure to E_2 and xenoestrogens during the developmental stage results in a marked influence on the generation of neuronal circuitry and vulnerability through unidentified mechanisms other than ERs. Although this influence can occur at very low concentrations (1 p*M* to 1 n*M*), its impact on the nervous systems of humans and animals cannot be elucidated at present. Risk assessment and, if applicable, development of procedures to overcome it may be necessary.

Acknowledgments

We thank Dr. Kawanishi for helpful advice on fluorescence measurements, and M. Tamuki for contributing to some experiments. This work was supported by a Health Science Research Grant for Research on Environmental Health and a Grant for 'Nano-medicine' Project from the Ministry of Health, Labor and Welfare, Japan.

References

1 Guillette EA, Meza MM, Aquilar MG, Soto AD, Garcia IE: An anthropological approach to the evaluation of preschool children exposed to pesticides in Mexico. Environ Health Perspect 1998;106:347–353.
2 Woolley CS, McEwen B: Estradiol regulates hippocampal dendritic spine density via an N-methyl-*D*-aspartate receptor-dependent mechanism. J Neurosci 1994;14:7680–7687.
3 Weiland NG: Estradiol selectively regulates agonist binding sites on the N-methyl-*D*-aspartate receptor complex in the CA1 region of the hippocampus. Endorcinology 1992;131:662–668.
4 Foy MR, Xu J, Xie X, Brinton RD, Thompson RF, Berger TW: 17β-estradiol enhances NMDA receptor-mediated EPSPs and long-term potentiation. J Neurophysiol 1999;81:925–929.
5 Wong M, Moss RL: Long-term and short-term electrophysiological effects of estrogen on the synaptic properties of hippocampal CA1 neurons. J Neurosci 1992;12:3217–3225.
6 Gu Q, Korach KS, Moss RL: Rapid action of 17β-estradiol on kainate-induced currents in hippocampal neurons lacking intracellular estrogen receptors. Endocrinology 1999;140:660–666.
7 Beyer C, Raab H: Nongenomic effects of oestrogen: Embryonic mouse midbrain neurons respond with a rapid release of calcium from intracellular stores. Eur J Neurosci 1998;10:255–262.
8 Mermelstein PG, Becker JB, Surmeier DJ: Estradiol reduces calcium currents in rat neostriatal neurons via a membrane receptor. J Neurosci 1996;16:595–604.
9 Stoppini L, Buchs PA, Muller DA: A simple method for organotypic cultures of nervous tissue. J Neurosci Methods 1991;37:173–182.
10 Zimmer J, Gahwiler BH: Cellular and connective organization of slice cultures of the rat hippocampus and fascia dentata. J Comp Neurol 1984;228:432–446.
11 Kirino T: Delayed neuronal death. Neuropathology 2000;20(suppl):S95–S97.
12 Sato K, Matsuki N: A 72-kDa heat shock protein is protective against the selective vulnerability of CA1 neurons and is essential for the tolerance exhibited by CA3 neurons in the hippocampus. Neuroscience 2002;109:745–756.
13 Nakagami Y, Saito H, Matsuki N: The regional vulnerability to blockade of action potentials in organotypic hippocampal culture. Brain Res Dev Brain Res 1997;103:99–102.
14 Sakaguchi T, Okada M, Kawasaki K: Sprouting of CA3 pyramidal neurons to the dentate gyrus in rat hippocampal organotypic cultures. Neurosci Res 1994;20:157–164.
15 Frederickson DJ, Kasarskis EJ, Ringo D, Frederickson RE: A quinoline fluorescence method for visualizing and assaying the histochemically reactive zinc (bouton zinc) in the brain. J Neurosci Methods 1987;20:91–103.
16 Nishikawa J, Saito K, Goto J, Dakeyama J, Matuso M, Nishihara T: New screening methods for chemicals with hormonal activities using interaction of nuclear hormone receptor with coactivator. Toxicol Appl Pharmacol 1999;154:76–83.
17 Kuiper GGJM, Carlsson B, Grandien K, Enmark E, Haggblad J, Nilsson S, Gustafsson J-A: Comparison of the ligand binding specificity and transcript tissue distribution of estrogen receptors α and β. Endocrinology 1997;138:863–870.
18 Monyer H, Sprengel R, Schoepfer R, Herb A, Higuchi M, Lomeli H, Burnashev N, Sakmann B, Seeburg PH: Heteromeric NMDA receptors: Molecular and functional distinction of subtypes. Science 1992;256:1217–1221.
19 Nakanishi S: Molecular diversity of glutamate receptors and implications for brain function. Science 1992;258:589–603.

20 Watanabe M, Fukaya M, Sakimura K, Manabe T, Mishina M, Inoue Y: Selective scarcity of NMDA receptor channel subunits in the stratum lucidum (mossy fibre-recipient layer) of the mouse hippocampal CA3 subfield. Eur J Neurosci 1998;10:478–487.
21 Germain SJ, Campbell PS, Anderson JN: Role of the serum estrogen-binding protein in the control of tissue estradiol levels during postnatal development of the female rat. Endocrinology 1978;103:1401–1410.
22 Hyder SM, Chiappetta C, Stancel GM: Triphenylethylene antiestrogens induce uterine vascular endothelial growth factor expression via their partial estrogen agonist activity. Cancer Lett 1997;120:165–171.
23 Singer CA, Rogers KL, Strickland TM, Dorsa DM: Estrogen protects primary cortical neurons from glutamate toxicity. Neurosci Lett 1996;212:13–16.
24 Kuiper GGJM, Lemmen JG, Carlsson B, Corton JC, Safe SH, Saag PT: Interaction of estrogenic chemicals and phytoestrogens with estrogen receptor β. Endocrinology 1998;139:4252–4263.
25 Wise PM, Dubal DB, Wilson ME, Rau SW, Bottner M, Rosewell KL: Estradiol is a protective factor in the adult and aging brain: Understanding of mechanisms derived from in vivo and in vitro studies. Brain Res Brain Res Rev 2001;37:313–319.
26 Goodman Y, Bruce A, Cheng B, Mattson MP: Estrogens attenuate and corticosterone exacerbates excitotoxicity, oxidative injury, and amyloid β-peptide toxicity in hippocampal neurons. J Neurochem 1996;66:1836–1844.
27 Kuroki Y, Fukushima K, Kanda Y, Mizuno K, Watanabe Y: Neuroprotection by estrogen via extracellular signal-regulated kinase against quinolinic acid-induced cell death in the rat hippocampus. Eur J Neurosci 2001;13:472–476.
28 Solum DT, Hand RJ: Estrogen regulates the development of brain-derived neurotrophic factor mRNA and protein in the rat hippocampus. J Neurosci 2002;22:2650–2659.
29 Moosmann B, Behl C: The antioxidant neuroprotective effects of estrogens and phenolic compounds are independent from their estrogenic properties. Proc Natl Acad Sci USA 1999;96:8867–8872.
30 Vergun O, Sobolevsky AI, Yelshansky MV, Keelan J, Khodorov BI, Duchen MR: Exploration of the role of reactive oxygen species in glutamate neurotoxicity in rat hippocampal neurons in culture. J Physiol 2001;531:147–163.
31 Sattler R, Tymianski M: Molecular mechanisms of glutamate receptor-mediated excitotoxic neuronal cell death. Mol Neurobiol 2001;24:107–129.
32 Gazzaley AH, Weiland NG, McEwen BS, Morrison JH: Differential regulation of NMDAR1 mRNA and protein by estradiol in the rat hippocampus. J Neurosci 1996;16:6830–6838.
33 Ramon Y, Cajal S: New Ideas on the Structure of the Nervous System in Man and Vertebrates (in French). Cambridge, MIT Press, 1990.
34 Shankaranarayana Rao BS, Raju TR, Meti BL: Self-stimulation rewarding experience induced alterations in dendritic spine density in CA3 hippocampal and layer V motor cortical pyramidal neurons. Neuroscience 1999;89:1067–1077.
35 McEwen BS, Tanapat P, Weiland NG: Inhibition of dendritic spine induction on hippocampal CA1 pyramidal neurons by a nonsteroidal estrogen antagonist in female rats. Endocrinology 1999;140:1044–1047.
36 Murphy DD, Segal M: Morphological plasticity of dendritic spines in central neurons is mediated by activation of cAMP response element binding protein. Proc Natl Acad Sci USA 1997;94:1482–1487.
37 Murphy DD, Cole NB, Greenverger V, Segal M: Estradiol increases dendritic spine density by reducing GABA neurotransmission in hippocampal neurons. J Neurosci 1998;18:2550–2559.
38 Wenzel HJ, Cole TB, Born DE, Schwartzkroin PA, Palmiter RD: Ultrastructural localization of zinc transporter-3 (ZnT-3) to synaptic vesicle membranes within mossy fiber boutons in the hippocampus of mouse and monkey. Proc Natl Acad Sci USA 1997;94:12676–12681.
39 Cole TB, Wenzel HJ, Kafer KE, Schwartzkroin PA, Palmiter RD: Elimination of zinc from synaptic vesicles in the intact mouse brain by disruption of the *ZnT3* gene. Proc Natl Acad Sci USA 1999;96:1716–1721.
40 Schacter D: The fluorometric estimation of magnesium in serum and urine. J Lab Clin Med 1959;54:763–768.
41 Watanabe S, Frantz W, Trottier D: Fluorescence of magnesium-, calcium-, and zinc-8-quinolinol complexes. Anal Biochem 1963;5:345–359.
42 Ribak CE, Baram TZ: Selective death of hippocampal CA3 pyramidal cells with mossy fiber afferents after CRH-induced status epilepticus in infant rats. Brain Res Dev Brain Res 1996;91:245–251.
43 Ben-Ari Y, Represa A: Brief seizure episodes induce long-term potentiation and mossy fibre sprouting in the hippocampus. Trends Neurosci 1990;13:312–318.
44 Represa A, Ben-Ari Y: Kindling is associated with the formation of novel mossy fibre synapses in the CA3 region. Exp Brain Res 1992;92:69–78.
45 Sperber EF, Stanton PK, Haas K, Ackermann RF, Moshe SL: Developmental differences in the neurobiology of epileptic brain damage. Epilepsy Res Suppl 1992;9:67–81.
46 Kossel AH, Williams CV, Schweizer M, Kater SB: Afferent innervation influences the development of dendritic branches and spines via both activity-dependent and non-activity-dependent mechanisms. J Neurosci 1997;17:6314–6324.
47 Maletic-Savatic M, Malinow R, Svoboda K: Rapid dendritic morphogenesis in CA1 hippocampal dendrites induced by synaptic activity. Science 1999;283:1923–1927.
48 McKinney RA, Capogna M, Durr R, Gahwiler BH, Thompson SM: Miniature synaptic events maintain dendritic spines via AMPA receptor activation. Nat Neurosci 1999;2:44–49.
49 Gu Q, Moss RL: 17β-estradiol potentiates kainate-induced currents via activation of the cAMP cascade. J Neurosci 1996;16:3620–3629.

HIGH-PRESSURE MEDIATED ASYMMETRIC DIELS-ALDER REACTION OF CHIRAL SULFINYLACRYLATE DERIVATIVES AND ITS APPLICATION TO CHIRAL SYNTHESIS OF (–)-COTC AND (–)-GABOSINE C[†]

Tamiko Takahashi,* Yoko Yamakoshi,[‡] Kazuya Okayama, Junko Yamada, Wei-Ying Ge, and Toru Koizumi[§]
Faculty of Pharmaceutical Sciences, Toyama Medical & Pharmaceutical University, 2630 Sugitani, Toyama 930-0194, Japan

Abstract – The asymmetric Diels-Alder reactions of chiral sulfinylacrylate derivatives (**1** and **2**) with dienes (**3–12**) were examined under high-pressure (1.2 GPa) conditions. The *endo* cycloadduct (**13e**) obtained from sulfinyl acrylate (**1**) and 2-methoxyfuran (**5**) was converted to (–)-COTC (**25**) and (–)-gabosine C (**26**).

The asymmetric Diels-Alder (D-A) reaction is one of the most efficient tools for constructing optically active cyclic compounds bearing up to four stereogenic centers in a single operation.[1] In a large number of highly asymmetric D-A reactions, there are numerous examples of cycloadditions of chiral dienophiles with active dienes such as cyclopentadiene.[2] Although considerable effort has been devoted to designing powerful chiral dienophiles which react with less active dienes such as furans, there are few successful examples of such cycloadditions.[3] Having negative volume of activation, D-A reaction is amenable to high-pressure conditions.[4] Moreover, high-pressure techniques have been known to be an efficient method not only for the synthesis of molecules sensitive to Lewis acid catalysis but also for enhancement of asymmetric induction.[5] Applying this technique, asymmetric D-A reactions would proceed without a Lewis acid between unactivated dienophiles and less active dienes,[6] and this strategy could have wide application. In a previous report,[7] we demonstrated high-pressure mediated asymmetric D-A reaction of chiral sulfinylacrylate derivatives (**1**[8] and **2**) with furan (**4**) or 2-methoxyfuran (**5**). We wish to report here the scope and limitations of this method and the application of the cycloadduct (**13e**) to the chiral synthesis of a glyoxalase I inhibitor, (–)-COTC (**25**)[3c,9] and (–)-gabosine C (antibiotic KD16-U1) (**26**)[10] in detail.

(+)-*Z*-3-(2-*exo*-Hydroxy-10-bornyl)propenamide (**2**) was prepared in two steps from 10-mercapto-2-*exo*-borneol[8] by successive Michael addition to propiolamide[11] and selective *m*CPBA oxidation in 43% overall yield. In order to establish the scope and limitations of high-pressure mediated asymmetric D-A reaction of the dienophiles (**1** and **2**), we investigated this reaction with various non-activated dienes (**4–7**, **9–12**) and with Danishefsky's diene (**8**) (Figure 1).

In our preliminary experiments, the steric course of the cycloaddition of **1** and **2** with cyclopentadiene (**3**) under high-pressure conditions was compared with that under atmospheric pressure conditions (Figures 1

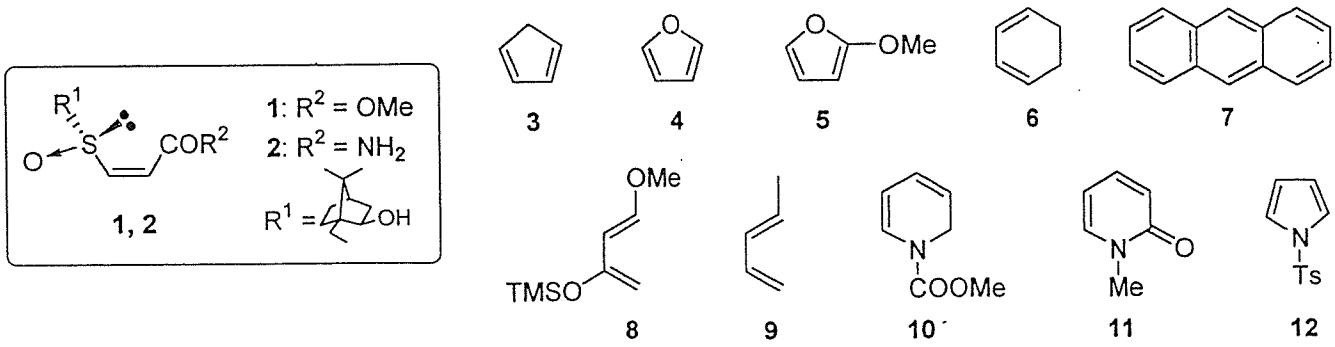

Figure 1

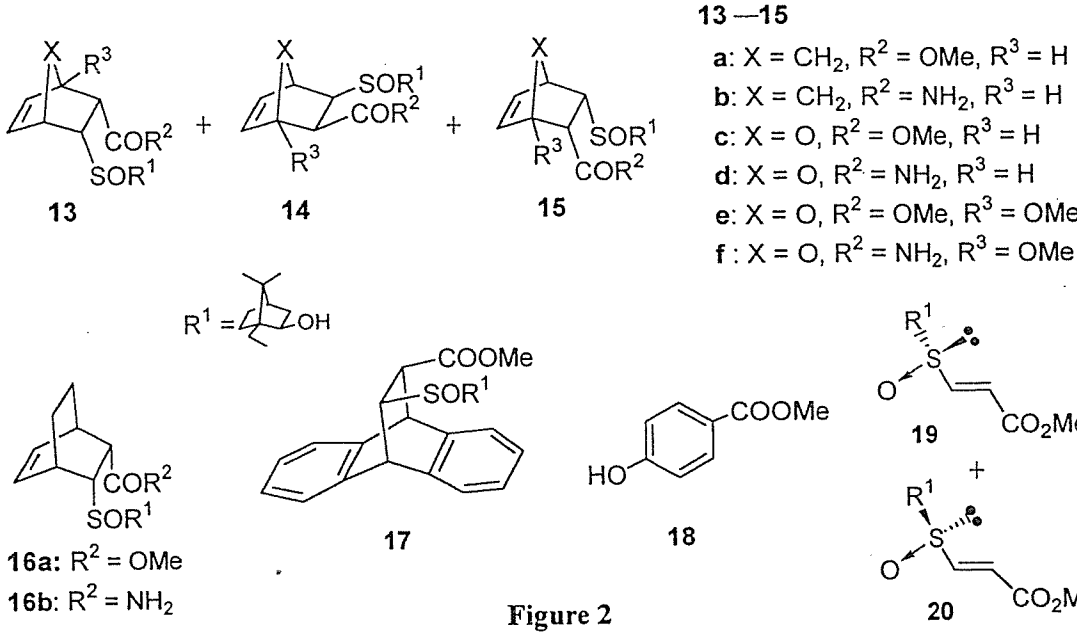

Figure 2

and 2). Reactions of **1** with **3** in CH_2Cl_2 proceeded readily at rt under both atmospheric and high-pressure (1.2 GPa) conditions to give the same *endo* cycloadduct **(13a)** as a single diastereomer in 92 and 88% yields, respectively. Similar reactions of **2** with **3** in CH_2Cl_2/MeOH (1:1) under atmospheric or high-pressure conditions gave *endo* cycloadduct **(13b)** and *exo* cycloadduct **(14b)** in 87 and 5% yields or 81 and 9% yields, respectively. All of these reactions proceeded with high diastereoselectivity and regioselectivity. The structure of **13a** was confirmed by comparison of its spectral data with those in the literature[8] and the absolute configuration of product **(13b)** was determined by X-Ray diffraction analysis. From these results, the same steric course was suggested for the reaction of **1** or **2** with **3** under both atmospheric and high-pressure conditions.[3b–e] The conformation for C=C–S=O of **1** and **2** should be oriented *s-trans* due to strong dipole-dipole repulsion between sulfinyl and carbonyl groups. An attack of **3** from the less hindered face (lone pair-side) is favored to give adducts **(13a,b)** (Figure 3).

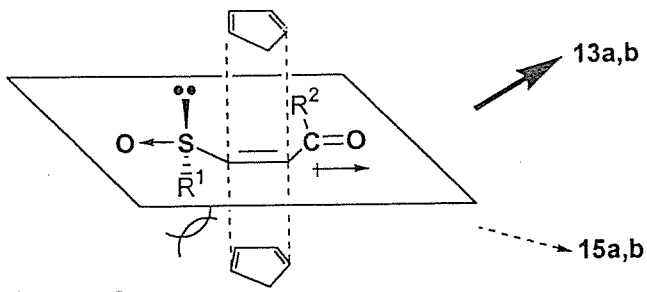

Figure 3

Most of the attempts to achieve the D-A reactions of dienophiles **(1** and **2)** with dienes **(4–12)** under thermal conditions (50–100 °C) were unsuccessful and the starting dienophiles were recovered. Reactions

of **1** with **6** and **8** in CH_2Cl_2 at 50 °C for 3 days in a sealed tube gave cycloadduct **(16a)** (9% yield) and methyl 4-hydroxybenzoate **(18)**[12] (8% yield), respectively. The adduct of **1** with **8** was not stable under the reaction conditions, and decomposed by spontaneous elimination of sulfenic acid and methanol as well as desilylation to afford **18**. In the presence of $ZnCl_2$, a sluggish reaction was observed between **1** and **6** to give **16a** (33% yield) at 70 °C after 4 days, whereas no reaction proceeded at all in the cases of **1** with **7** and **9–12**. In contrast, D-A reaction took place under high-pressure (1.2 GPa) conditions. The most significant results are summarized in Table 1. The high-pressure reaction conditions proved to be very effective for asymmetric D-A reactions of **1** and **2** with dienes **(4–7)** in respect of diastereoselectivity (from 95:5 to 100:0) and regioselectivity (from 71:29 to 100:0) giving the cycloadducts **(13–17)** (entries 1–7). Due to lower reactivity of the amide **2**, the diastereoselectivity of the reactions of **2** may be higher than that of the ester **1**. The configuration of *endo* and *exo* cycloadducts **(13–16)** was deduced by ^{1}H-NMR spectra and mechanistic consideration.[3b–e] Reaction of **1** with **8** gave **18** in low yield (entry 8). In the reaction of **1** with **9**, only isomerized dienophiles **19**[13] and **20**[13] were obtained (entry 9). All reactions of **2** with **7–12** as well as of **1** with **10–12** did not occur at all. From these results, high-pressure mediated conditions are proved to be especially suited for the asymmetric D-A reaction of the dienophiles (**1** and **2**) with furans (**4** and **5**).

Table 1. High-Pressure (1.2 GPa) Mediated Asymmetric D-A Reactions of Chiral Sulfinylacrylate Derivatives (**1** and **2**) with Dienes (**4–9**)

			reaction conditions				
entry	dienophile	diene	temp.	solv.[a]	time (days)	products (ratio)[b]	yield (%)
1	**1**	**4**	rt[c]	A	3	**13c/14c/15c** (82:14:4)	94
2	**2**	**4**	rt[c]	B	3	**13d** (100)	81
3	**1**	**5**	rt[c]	A	3	**13e/14e** (71:29)	d
4	**2**	**5**	rt[c]	B	3	**13f/14f** (92:8)	e
5	**1**	**6**	50 °C	A	3	**16a**	32
6	**2**	**6**	50 °C	B	7	**16b**	28
7	**1**	**7**	80 °C	A	7	**17**	13
8	**1**	**8**	80 °C	A	3	**18**	18
9	**1**	**9**	50 °C	A	7	**19/20** (85:15)	26

a) A: CH_2Cl_2; B: CH_2Cl_2/MeOH (1:1). b) Ratios were determined by ^{1}H-NMR spectroscopy. c) Rt. d) Because of its instability, **13e** was isolated as diol **(21e)** after dihydroxylation (53% yield from **1**). e) Because of its instability, **13f** was isolated as diol **(21f)** after dihydroxylation (63% yield from **2**).

In order to confirm the absolute configuration of major *endo* adduct **(13)**, **13e** was converted to (–)-COTC **(25)** and gabosine C **(26)** (Scheme 1). Dihydroxylation of **13e** afforded diol **(21e)** (53% yield from **1**). Acetonide formation of **21e** gave **22** (64% yield). Reaction of **22** with $LiAlH_4$ afforded alcohol **(23)** which was esterified with crotonic anhydride to give **24** (43% yield from **22**). Treatment of **24** with trifluoroacetic acid (TFA) afforded (–)-COTC **(25)** (29% yield). Likewise, treatment of **23** with TFA gave

(–)-gabosine C **(26)** (51% yield from **22**). ^{1}H-NMR and IR spectra of **25** and **26** were identical with those reported.[3c,9,10] From these results, the absolute configuration of **13e** was determined as shown in Figure 2

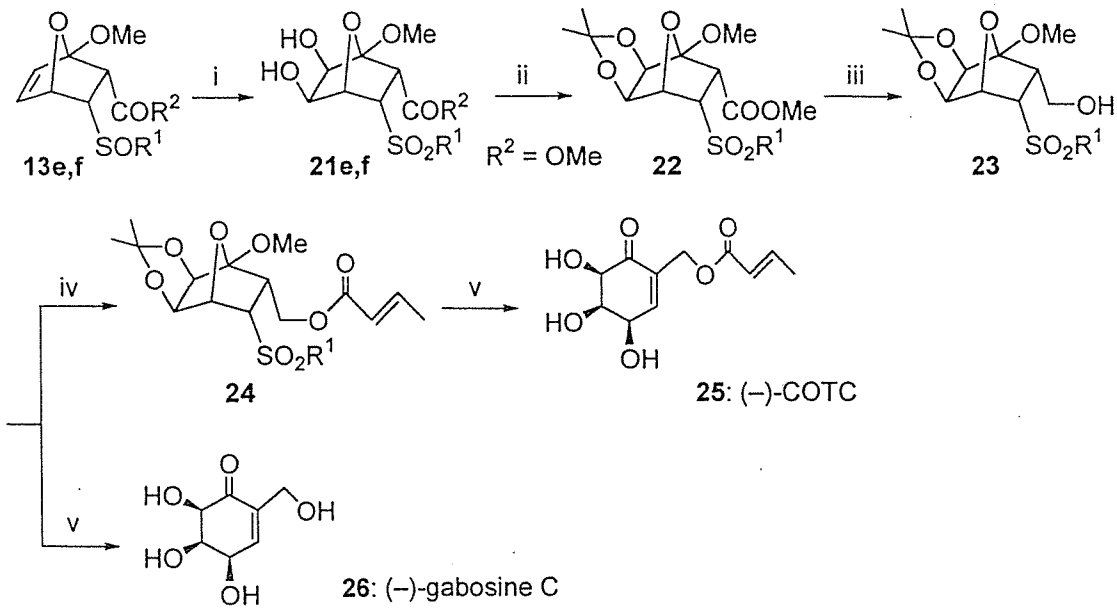

i) cat. OsO_4, Me_3NO, acetone, 0 °C then rt, **21e**: 53% from **1**, **21f**: 63% from **2**; ii) 2,2-dimethoxypropane, cat. *p*-TsOH, acetone, reflux, 64%; iii) $LiAlH_4$, THF, rt; iv) crotonic anhydride, pyridine, DMAP, benzene, rt, 43% from **22**; v) 80% aqueous TFA, –20 °C, **25**: 29%, **26**: 51% from **22**.

Scheme 1

and Scheme 1. Accordingly, the steric course of the reaction was confirmed to be the same in these asymmetric cycloadditions under both atmospheric and high-pressure conditions.

In conclusion, we have successfully developed high-pressure mediated asymmetric D-A reaction of unactivated dienophiles, sulfinylacrylate derivatives (**1** and **2**), with less active dienes. This technique proved to be very effective for combination of **1** and **2** with the dienes (**4**–**7**) in respect of diastereoselectivity and regioselectivity. However, the dienes (**8**–**12**) were not suited for this reaction. Transformation of the major *endo* adduct (**13e**) to (–)-COTC (**25**) and (–)-gabosine C (**26**) provided not only determination of the absolute configuration of **13e** but also a new strategy for a chiral synthesis of natural polyoxygenated cyclohexane derivatives.

EXPERIMENTAL

Melting points were measured with a Yanaco micro melting point apparatus and are uncorrected. Microanalyses were performed by Microanalysis Center of Toyama Medical & Pharmaceutical University. Spectroscopic measurements were carried out with the following instruments: optical rotations, JASCO DIP-1000 digital polarimeter; IR, Perkin-Elmer 1600 Series FTIR; ^{1}H-NMR, Varian Gemini 300 (300 MHz) and Varian Unity 500 (500 MHz) for solutions in $CDCl_3$, $CDCl_3/CD_3OD$ or CD_3OD with Me_4Si as internal standard; ^{13}C-NMR, Varian Gemini 300 (75 MHz) for solutions in CD_3OD with Me_4Si as internal standard; MS and HRMS spectra, JEOL JMS D-200 and JEOL JMS AX-505H. High-pressure reactions were carried out by using an ordinary high-pressure apparatus. Column chromatography, flash column chromatography, and preparative TLC (PLC) were performed on Kieselgel 60 (Merck, Art. 7734, Art. 9385 and Art. 7748, respectively) and cellulose (Merck, Art. 15275).